*Desalination and Water Treatment*
www.deswater.com
doi: 10.5004/dwt.2023.29559

294 (2023) 139–148
May

# Strontium removal from aquatic solution using electric arc furnace slag: kinetic, equilibrium and thermodynamic approach

Milena Tadić[a], Irena Nikolić[a], Nevana Cupara[b], Dijana Djurović[b,*], Ivana Milašević[b]

[a]*Faculty of Metallurgy and Technology, University of Montenegro, Džordža Vašingtona bb, 81000 Podgorica, Montenegro, emails: milenak@ac.me (M. Tadić), irena@ucg.ac.me (I. Nikolić)*
[b]*Institute of Public Health of Montenegro, Džona Džeksona bb, 81000 Podgorica, Montenegro, emails: dijana.djurovic@ijzcg.me (D. Djurović), ncupara@ymail.com (N. Cupara), ivanamilasevic@gmail.com (I. Milašević)*

Received 1 December 2022; Accepted 3 April 2023

**ABSTRACT**

This study investigated strontium removal from aqueous solution using electric arc furnace (EAF) slag. Influence of sorbent dosage (0.5–3 g/L), pH (2.5–9.5), initial concentration of $Sr^{2+}$ (50–300 ppm) and temperature (20°C–45°C) was evaluated. Optimal sorbent dosage and initial $Sr^{2+}$ concentration were found to be 1.5 g/L and 150 ppm, respectively. Kinetics, equilibrium and thermodynamic models were used to analyse the data. Kinetics of $Sr^{2+}$ adsorption onto EAF slag was evaluated using pseudo-first-order and pseudo-second-order models and results have shown that experimental data had a better fit with the pseudo-second-order model. Langmuir and Freundlich isotherm models were used for evaluating the adsorption equilibrium and it has been shown that Langmuir model better described isotherm data. Maximal adsorption capacities of 111.11, 129.87 and 156.25 mg/g were obtained at 20°C, 30°C and 45°C, respectively. Thermodynamic investigation indicated that adsorption of $Sr^{2+}$ onto EAF slag is endothermic in nature, spontaneous and more favorable at higher temperatures.

*Keywords:* Electric arc furnace slag; Strontium; Adsorption; Kinetics; Equilibrium; Thermodynamics

## 1. Introduction

One of the biggest problems of nuclear waste management is the disposal of radioactive wastewater whose detrimental effects on the environment and human health is well known. Radioactive wastewaters mainly contain isotopes of elements such as strontium, cesium, plutonium, americium and technetium [1]. Strontium is a persistent radionuclide in the environment [2], characterised by high solubility, biotoxicity and long shelf life [1]. It is also present in high levels in liquid waste generated by the reprocessing of spent nuclear fuel [3,4]. Thus, separation of strontium from waste solutions requires special attention.

Chemical precipitation and flocculation [5], membrane process [6], ion exchange [7,8], immobilization method [9] and adsorption were mainly investigated for removal of radioactive ions from wastewater. However, adsorption has been proposed as a cost-efficient method for removing heavy metals from wastewaters due to a variety of available low-cost adsorbents. Various adsorbents were used for the removal of radionuclide from wastewaters such as: natural and synthetic zeolites [10], natural clinoptilolite [11], binary mineral mixtures of montmorillonite and kaolinite [12], multiwall carbon nanotube/iron oxide magnetic composites [13,14], composite magnetic particles derived from $Fe_3O_4$ and bis (trimethoxysilylpropyl) amine [15], activated carbon [16], etc.

Utilization of solid industrial waste as adsorbents for removal of different pollutants from wastewater has recently attracted special attention [17]. Use of waste material from

* Corresponding author.

steel production is of extremely importance considering its abundance. Steel production in 2021 was 1,950.5 million tonnes with about 30% of steel produced via electric arc furnaces which utilize electricity to melt steel scrap [18]. This waste material is known as electric arc furnace slag (EAF slag) and currently there is an increasing interest in the valorization of slag since its annual production in the European Union in 2018 was around 16.3 million tonnes, about 31% of which was produced by EAF route [19]. EAF slag, which is characterized as non-hazardous waste, is formed during the melting process and floats on the surface of molten steel, protecting it from oxidation. This slag mainly comprises of Fe, Ca, Si, Al and Mg based oxides, where the content depends on the compositions of scrap charged into the furnaces as well as the processing conditions [20].

Electric furnace slag has numerous valorization possibilities for metallurgical as well as non-metallurgical purposes. Valorization of EAF slag for metallurgical purposes is based on metal extraction, while for non-metallurgical purposes this slag is mainly used in construction (road construction). However, an important shift was made towards the application of for wastewaters treatment. Successful application of EAF slag for heavy metals removal from wastewaters was reported [21–23]. Adsorption properties of slag may be improved by slag leaching with demineralized water [24], treatment with $Na_2SiO_3$ solution and dimethyl silicone oil and thermal treatment [25] as well as by slag surface modification through alkali activation process [26].

Although radioactive wastewaters loaded with strontium are not the only source of environmental pollution but also wastewaters from oil exploration drilling and its application in flares and fireworks, paints and plastics, and medicine [27], $Sr^{2+}$ adsorption from wastewaters so far has not received proper attention. Research in this field was mainly directed towards the usage of natural materials like kaolinite [28] and dolomite [29]as well as some other adsorbents including three-dimensional barium sulfate-impregnated reduced graphene oxide (rGO) aerogel [30], ethylenediamine triacetic acid (EDTA) functionalized graphene oxide [31], graphene oxide-hydroxyapatite nanocomposite [32], magnetite nanoparticles decorated rGO composite [33], synthesized oxide materials [34], chemically synthesized zeolite [35], synthetic hydroxyapatite [36]. However, the high synthesis cost of these materials limits their application.

To the best of our knowledge there is no data on the usage of low-cost adsorbent based on industrial waste for $Sr^{2+}$ removal from wastewaters. Thus, the novelty of this research includes comprehensive kinetics, equilibrium and thermodynamic evaluation of the adsorption of $Sr^{2+}$ onto industrial waste material (EAF slag) together with microstructural characterization of sorbent in order to further understand the adsorption process mechanism.

## 2. Experimental

### 2.1. Sorbent characterisation techniques

Sorbent (EAF slag) used in this research was supplied from the Still Mill in Montenegro. Chemical composition of the slag is given in Table 1.

Prior to the adsorption experiment, EAF slag was grounded to a powder and washed by acid and deionized water [37] and particle size was determined using a laser particle size analyser (Mastersizer 2000, Malvern Instruments Ltd., United Kingdom). ASAP 2020 instrument was used to evaluate porosity with specific surface area and pore volume of sorbent determined by Brunauer–Emmett–Teller (BET) [38] and Barrett–Joyner–Halenda (BJH) [39] methods, respectively.

The sorbent sample was additionally subjected to X-ray powder diffraction (XRPD) analysis and scanning electron microscopy (SEM). The XRPD data was collected on a Rigaku RINT-TTRIII diffractometer (Rigaku Europe SE, Hugenottenallee 167, Neu-Isenburg 63263, Germany), with Cu-K$\alpha$ radiation of $\lambda$ = 1.5406 Å at room temperature in the $2\theta$ range of 10°–70° with a scanning step of 0.02° and scan speed of 5 s per step.

Microstructural investigations were carried out using the FEI DB235 focused ion beam system, equipped with an energy-dispersive X-ray spectrometer (EDS). The SEM images were recorded with various electron detectors, including the secondary electron detector.

Point of zero charge ($pH_{pzc}$) in sorbent sample was evaluated by batch equilibrium method [40] with $KNO_3$ solution (0.1 mol/L) was used as the background electrolyte. The pH of initial solution ($pH_i$) was adjusted by addition of $HNO_3$ (0.1 mol/L) or KOH (0.1 mol/L). The amount of 0.1 g of sample was added into the 50 mL of each initial solution and shaken for a 24 h at room temperature, centrifuged and the pH of supernatants was determined ($pH_f$). The point of zero charge was determined as the pH value at which a plateau is obtained on the graph $(pH_f) = f(pH_i)$.

### 2.2. Batch adsorption experiments

The adsorption tests were carried out using synthetic solutions containing $Sr^{2+}$ ions since in Montenegro there is no industry which generates $Sr^{2+}$ loaded wastewaters and the attention is paid to the usage EAF slag as a sorbent. Adsorption experiments were carried out in batch conditions for 60 min at various adsorbent dosage (0.5, 1, 1.5, 2, 2.5 and 3), initial concentrations (50, 100, 150, 200, 250 and 300 ppm) and temperatures (20°C, 30°C and 45°C) at pH value of 5. Solutions containing $Sr^{2+}$ ions were prepared from analytical grade chemicals, $SrCl_2$ in deionized water. During the adsorption experiments, an aliquot of the suspension

Table 1
Chemical composition of electric arc furnace slag

| Component | % |
|---|---|
| CaO | 46.50 |
| FeO | 23.50 |
| $SiO_2$ | 12.21 |
| $Al_2O_3$ | 7.20 |
| MgO | 6.48 |
| MnO | 1.30 |
| $TiO_2$ | 1.06 |
| $Fe_2O_3$ | 0.91 |
| $Cr_2O_3$ | 0.82 |
| LOI | 4.25 |

*Loss on ignition

was taken at certain intervals of time, filtered and tested for the concentrations of metal ions using inductively coupled plasma optical emission spectrometry (ICP-OES).

Removal efficiency of $Sr^{2+}$ ions (RE) and adsorption capacity ($q_t$) at any given time were calculated according to Eqs. (1) and (2).

$$\mathrm{RE} = \frac{C_0 - C_t}{C_0} \times 100\% \quad (1)$$

$$q_t = \frac{\left(C_0 - C_t\right)}{m} V \quad (2)$$

where $C_0$ and $C_t$ are the initial and final concentrations of $Sr^{2+}$ ions in solution, respectively, $V$ is the volume of $Sr^{2+}$ ion solution and $m$ is the dry mass of adsorbent.

## 3. Results and discussion

### 3.1. Characterisation of sorbent

The results of particle size analysis have shown a narrow particle-size distribution of EAF slag (span = 2.04), where 10% of particles ($d(0.1)$) are smaller than 3.85 μm, 90% of particles ($d(0.9)$) are smaller than 23.6 μm and average particle size $d(0.5)$ was calculated to be 9.67 μm (Fig. 1a). The $pH_{pzc}$ of sorbent sample was found to be 4.3 (Fig. 1b).

The results of porosity analysis indicated mesoporous particles (pore diameters between 2 and 50 nm) since isotherms for EAF slag (Fig. 1c) are of type IV with a hysteresis loop. The curves of pore-size distribution indicate a unimodal pore-size distribution (inset in Fig. 1c). The sharp peak that reflects the majority of pores is observed at around 2.2 nm. The results of BET analysis of sorbent particles provided the following data: total pore volume 0.002199 $cm^3/g$, surface area 0.6 $m^2/g$, and the average pore diameter was found to be 12.1 nm.

The main crystal phases identified in sorbent (Fig. 1d) were larnite, $Ca_2SiO_4$ (COD ID 96-901-2790), wüstite, FeO (COD ID 96-101-1199), gehlenite, $Ca_2Al(AlSiO_7)$ (COD ID 96-100-0049), and monticellite, $CaMgSiO_4$ (COD ID96-900-1081). Spinel, $MgAl_2O_4$ (COD ID 96-900-2745) and calcite, $CaCO_3$ (COD ID 96-901-6180) phases were present in smaller quantities.

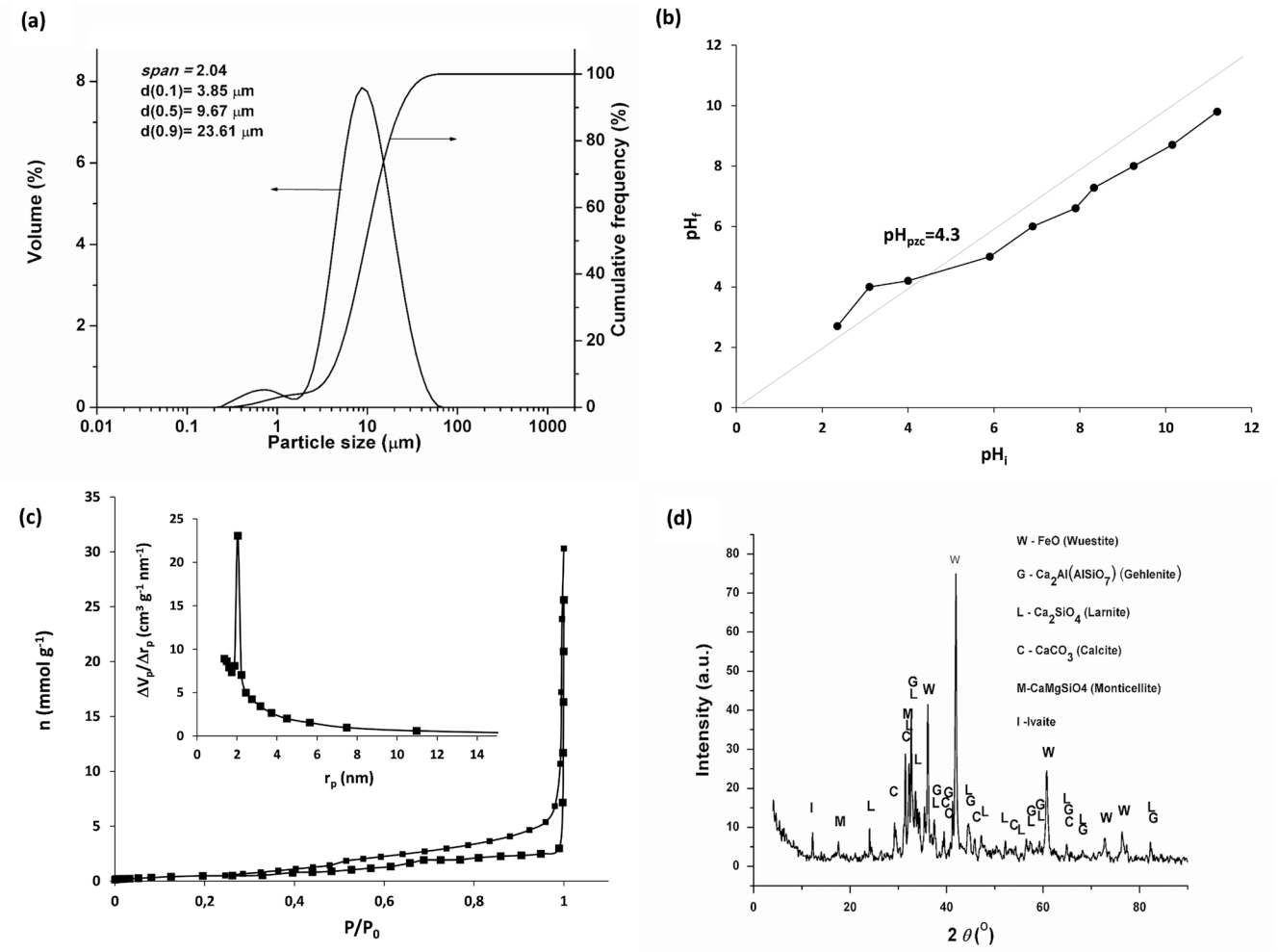


Fig. 1. Particle-size distribution of electric arc furnace slag based on particle number and cumulative percentage frequency (a), $pH_{pzc}$ of slag (b), adsorption/desorption isotherms and pore-size distribution of electric arc furnace slag (c), and XRPD of electric arc furnace slag (d).

*3.2. Effect of sorbent dosage and initial concentration of $Sr^{2+}$ ions*

Effect of adsorbent dosage was investigated in the range between 0.5–3 g/L keeping the initial metal concentration of 150 ppm and temperature of 20°C constant (Fig. 2a). Increase of adsorbent dosage in the range of 0.5–1.5 g/L lead to the rise of removal efficiency with the maximum achieved at solid to liquid (S/L) ratio of 1.5 while a further increase of S/L ratio lead to the efficiency decrease. Increase of $Sr^{2+}$ removal from aquatic solution in the range of 0.5–1.5 g/L dosage is attributed to the higher availability of adsorption site for metal binding [41]. Decline of removal efficiency with rising adsorbent dosage above 1.5 g/L is attributed to the excessive active sites on the adsorbent surface relative to the content of $Sr^{2+}$ in the solution [42]. Thus S/L ratio of 1.5 g/L was chosen as optimal for further investigation.

Influence of initial concentration of $Sr^{2+}$ ions on the removal efficiency from aquatic solution onto EAF slag is given in Fig. 2b. The rise of removal efficiency with the increase of initial metal concentration was observed in interval of 50–150 ppm which is followed by substantial decrease of removal efficiency with further increase of initial metal concentration from 150 to 300 ppm. Thus, the initial concentration of $Sr^{2+}$ of 150 ppm was chosen as optimal and set for the rest of experiments. The abundance of active sites on the sorbent surface is essential for the efficiency of metal removal from solution. Numerous active sites at the sorbent surface are available for metal sorption at low initial metal concentration in a solution which is accompanied by the efficient removal of metal ions from solution [42]. Moreover, an increase in the initial metal concentration leads to an increase in the probability of collisions between metal ions and active sites as a result of driving force the increase, necessary to overcome the resistance of metal ion mass transfer from aqueous to solid phase. Thus, removal efficiency from the solution increases [43,44]. However, at higher initial concentration, a fixed number of available active site is occupied and the excess of metal ions can't be adsorbed, leading to a drop in removal efficiency.

*3.3. Effect of pH*

Adsorption process is strongly influenced by the pH of the solution which influences the surface charge of the adsorbent. Influence of pH of solution on the Sr adsorption onto EAF slag is given in Fig. 3. It is evident that the increase of removal efficiency of $Sr^{2+}$ follows the rise of pH until the value of 5. Further rise of pH slightly affected $Sr^{2+}$ removal from solution and the pH value of 5 was chosen as optimal for further adsorption tests. The observed change in $Sr^{2+}$ removal efficiency is in accordance with the $pH_{pzc}$ value of 4.3. When the pH of solution was lower than $pH_{pzc}$, the surface of the adsorbent was positively charged, favoring the adsorption of anions on it while at pH higher than $pH_{pzc}$ the sorbent surface was negatively charged, and adsorption of cation was more favorable. Thus, at the pH above 4.3, the slag surface becomes negatively charged enhancing the $Sr^{2+}$ sorption while at the pH below the 4.3 adsorption of $Sr^{2+}$ was inhibited due to the presence of positively charged sorbent surface.

*3.4. Effect of contact time and temperature*

Adsorption of $Sr^{2+}$ from aquatic solution using EAF slag was investigated in the 2–35 min range at constant initial concentration of $Sr^{2+}$ (150 mg/L), adsorbent dosage (1.5 g/L) and pH of 5. The results are given in Fig. 4. The calculated removal efficiency of $Sr^{2+}$ within 35 min of adsorption at 20°C was 68.75% with a majority of $Sr^{2+}$ ions removed from

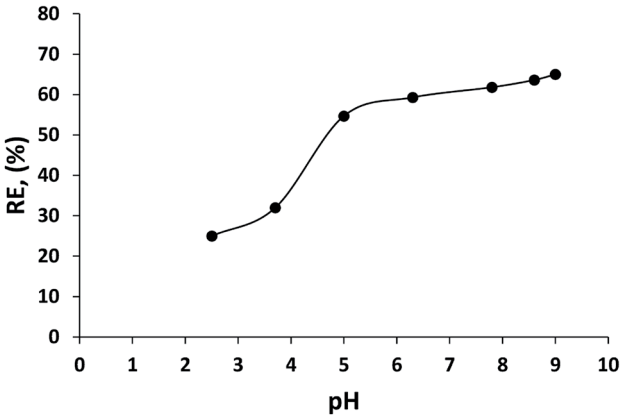


Fig. 3. Effect of pH on the adsorption of $Sr^{2+}$ by electric arc furnace slag.

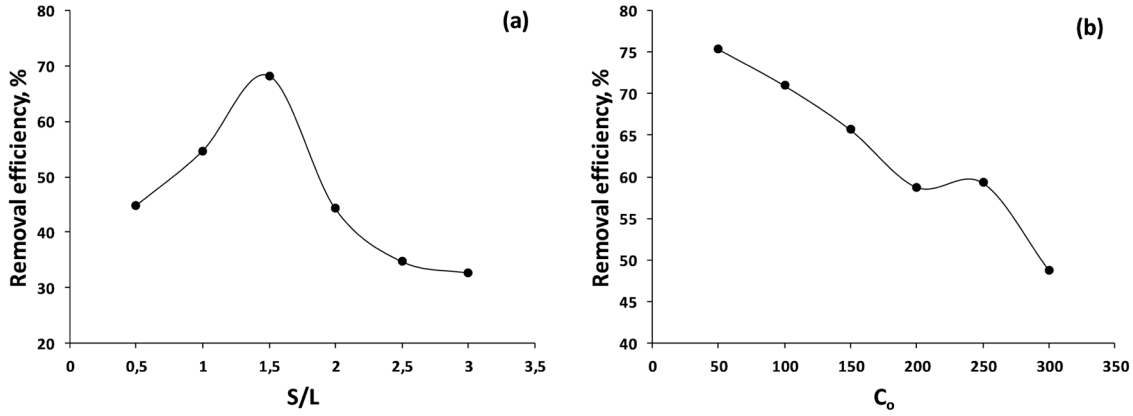


Fig. 2. Effect of adsorbent dosage (a) and (b) initial strontium concentration on the adsorption of $Sr^{2+}$ by electric arc furnace slag.

solution in the initial stage of adsorption due to the presence of a large number of available active sites. The major fraction of $Sr^{2+}$ was removed from solution by EAF slag within the first 15 min. Further prolongation of adsorption process practically had no influence on the $Sr^{2+}$ adsorption indicating that after 15 min, the equilibrium was reached. Increase of adsorption temperature to 35°C and 45°C was favorable for the adsorption of $Sr^{2+}$ onto EAF slag (Fig. 3) indicating endothermic character of $Sr^{2+}$ adsorption. The rise of temperature from to 35°C and 45°C increases the removal efficiency of $Sr^{2+}$ onto EAF slag to 75.93% and 88.40%, respectively.

### 3.5. Adsorption kinetics and equilibrium

Adsorption kinetics were evaluated using the pseudo-first-order and pseudo-second-order models, with integrated forms expressed by Eqs. (3) and (4), respectively:

$$\log\left(q_e - q_t\right) = \log q_e - \left(\frac{k_1}{2.303}\right)t \tag{3}$$

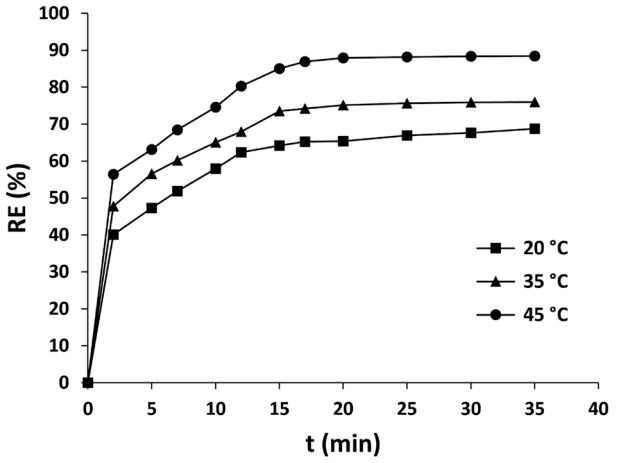


Fig. 4. Removal efficiency of $Sr^{2+}$ ions by electric arc furnace slag as a function of adsorption time.

$$\frac{t}{q_t} = \frac{t}{q_e} + \frac{1}{k_2 q_e^2} \tag{4}$$

where $q_e$ (mg/g), denotes adsorption capacity in equilibrium, $k_1$, ($min^{-1}$) and $k_2$, (g/mg·min) are rate constants of the pseudo-first-order sorption and pseudo-second-order sorption, respectively. When the pseudo-first-order model was applied, values of $k_1$ and $q_e$ were calculated from the slope and intercept of straight-line plots $\log(q_e - q_t)$ vs. $t$. In case of pseudo-second-order model, $k_2$ and $q_e$ were calculated from the intercept of and slope of the plot of $t/q_t$ vs. time.

The results of investigation of adsorption kinetic of $Sr^{2+}$ ions onto EAF slag are given in Fig. 5a and Table 2. Analysis of adsorption kinetics has shown that pseudo-second-order model is a better fit with experimental data since high regression coefficients ($R^2$) were obtained and calculated values of $q_e$ were in good agreement with the experimental values for $q_e$ (Table 2). The pseudo-second-order model

Table 2
Kinetics parameters for $Sr^{2+}$ adsorption onto electric arc furnace slag obtained using two kinetics models at three different temperatures

| Pseudo-first-order kinetic model | | | | |
|---|---|---|---|---|
| Temperature (°C) | $q_e$, experimental | $q_e$, calculated | $k_1$ | $R^2$ |
| 20 | 64.23 | 57.72 | 0.26 | 0.936 |
| 35 | 75.36 | 51.70 | 0.22 | 0.953 |
| 45 | 87.73 | 63.80 | 0.20 | 0.932 |
| Pseudo-second-order kinetic model | | | | |
| Temperature (°C) | $q_e$, experimental | $q_e$, calculated | $k_2 \times 10^{-3}$ | $R^2$ |
| 20 | 64.23 | 71.43 | 10.15 | 0.996 |
| 35 | 75.36 | 79.37 | 10.33 | 0.997 |
| 45 | 87.73 | 90.91 | 10.83 | 0.997 |

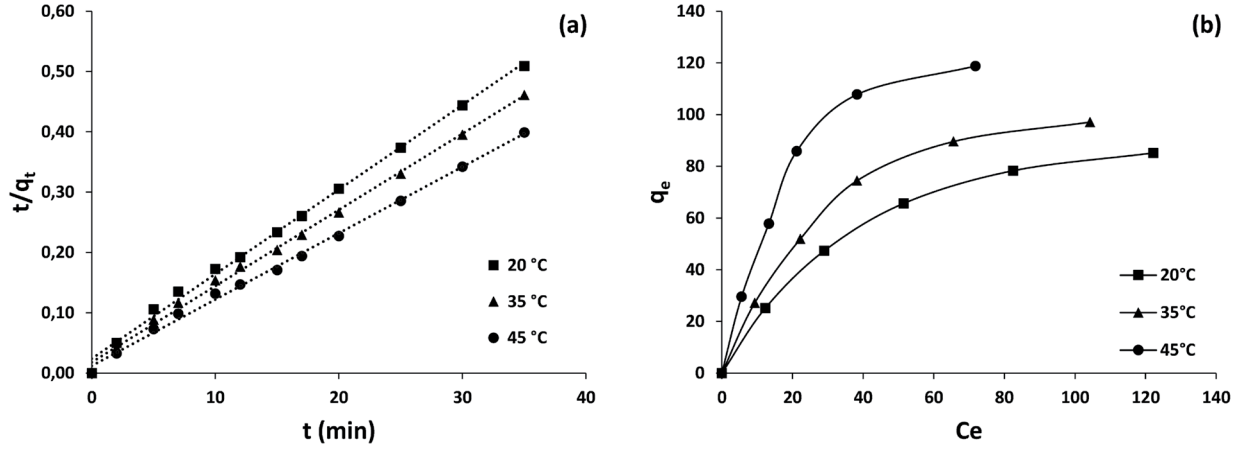


Fig. 5. Pseudo-second-order kinetics plots (a) and adsorption isotherms (b) of $Sr^{2+}$ onto electric arc furnace slag at different temperatures.

assumed the formation of chemisorptive bonds between the adsorbate and the adsorbent, that is, a chemical reaction is a rate controlling process [45,46].

Adsorption isotherm study was evaluated using Langmuir [Eq. (5)] and Freundlich [Eq. (6)] isotherm models:

$$\frac{C_e}{q_e} = \frac{C_e}{Q_0} + \frac{1}{Q_0 K_L} \tag{5}$$

$$\ln\left(q_e\right) = \ln\left(K_F\right) + \frac{1}{n}\ln\left(C_e\right) \tag{6}$$

where $C_e$ denoting equilibrium concentration of $Sr^{2+}$ ions, $Q_0$ (mg/g) as maximum adsorption capacity, $K_L$ (L/mg) as Langmuir adsorption constant related to the adsorption energy, $K_F$ (mg/g)(mg/L)$^{1/n}$ as Freundlich constant related to the adsorption capacity and $1/n$ as the constant related to the adsorption intensity of the adsorbent. Langmuir parameters, $Q_0$ and $K_L$ were obtained from the slope and intercept of plots $C_e/q_e$ while values for $K_F$ and $1/n$ were determined from the intercept and slope of $\ln(q_e)$ vs. $\ln(C_e)$ plots, respectively.

The affinity between $Sr^{2+}$ ions and adsorbents can be predicted using the Langmuir dimensionless separation factor $R_L$ [47] which is given by following equation:

$$R_L = \frac{1}{1 + K_L C_0} \tag{7}$$

The value of $R_L$ indicates the nature of the adsorption process, that is, whether it is irreversible ($R_L$ = 0), favorable ($0 < R_L < 1$), linear ($R_L = 1$) or unfavorable ($R_L > 1$).

Adsorption isotherms obtained for $Sr^{2+}$ adsorption onto EAF slag at different temperatures are presented in Fig. 5b and adsorption parameters are given in Table 3. It is evident that the increase of equilibrium concentration of $Sr^{2+}$ ions lead to the increase of adsorption capacity at all investigated temperatures. The results presented in Table 3 indicate that adsorption of $Sr^{2+}$ ions on the EAF slag obeys the Langmuir model (high correlation coefficient for Langmuir model $R^2 > 0.98$) suggesting that the adsorption of $Sr^{2+}$ occurs on a homogenous surface of EAF slag covered by a monolayer of the adsorbate. Moreover, increase of Langmuir isotherm parameters ($Q_0$ and $K_L$) with the increase of temperature indicates that the rise of temperature favors the adsorption process.

The values of Langmuir dimensionless separation factor $R_L$, which indicate the affinity between $Sr^{2+}$ and adsorbate, are given in Table 4. The results presented in Table 4 indicated the adsorption process as favorable since value of $R_L$ obtained at different initial concentration of $Sr^{2+}$ ions fall in the range $0 < R_L < 1$.

Comparison of maximum adsorption capacity for $Sr^{2+}$ adsorption obtained in this study (111.11 mg/g, at 20°C) with those obtained using different adsorbents reported in literature is given in Table 5 where the superiority is evident compared to dolomite, expanded perlite and metakaolin/slag-based zeolite microspheres (M/SZMs) geopolymer and hydroxyapatite embedded micro-adsorbents [29,42,48,49]. As expected, considerably lower $Sr^{2+}$ uptake was observed in comparison to materials with costly synthesis procedures such as graphene oxide, $BaSO_4$-rGO aerogel, EDTA functionalized graphene oxide, graphene oxide-hydroxyapatite nanocomposite and zeolitic materials [27,30–32,50]. The differences in adsorption capacities are atributed to the different surface properties and nature of functional groups present in different adsorbents.

### 3.6. Adsorption mechanism

Adsorption process involves three stadiums: film or external diffusion, intraparticle diffusion and adsorption of metal ions onto the active sites on the interior surfaces of adsorbent pores. In order to determinate which of these

Table 3
Adsorption isotherm parameters for $Sr^{2+}$ adsorption onto electric arc furnace slag

| Temperature (°C) | Langmuir isotherm | | | Freundlich isotherm | | |
|---|---|---|---|---|---|---|
| | $Q_0$ | $K_L$ | $R^2$ | $K_F$ | $n$ | $R^2$ |
| 20 | 111.11 | 0.026 | 0.995 | 91.54 | 1.85 | 0.963 |
| 35 | 129.87 | 0.031 | 0.993 | 162.29 | 1.86 | 0.949 |
| 45 | 156.25 | 0.049 | 0.987 | 367.79 | 1.79 | 0.929 |

Table 4
Values of $R_L$ for different initial concentration of $Sr^{2+}$ ions

| Concentration (ppm) | Temperature (°C) | | |
|---|---|---|---|
| | 20 | 35 | 45 |
| 50 | 0.436 | 0.392 | 0.292 |
| 100 | 0.279 | 0.244 | 0.171 |
| 150 | 0.205 | 0.2050 | 0.121 |
| 200 | 0.162 | 0.139 | 0.093 |
| 250 | 0.134 | 0.114 | 0.077 |

Table 5
Maximum adsorption capacity for $Sr^{2+}$ onto different absorbents

| Adsorbent | $Q_0$ (mg/g) | References |
|---|---|---|
| Electric arc furnace slag | 111.1 | This study |
| Graphene oxide | 131.4 | [27] |
| Dolomite | 1.172 | [29] |
| $BaSO_4$-rGO aerogel | 232.9 | [30] |
| EDTA functionalized graphene oxide | 172.3 | [31] |
| Expanded perlite | 1.14 | [48] |
| Graphene oxide-hydroxyapatite nanocomposite | 702.2 | [32] |
| Metakaolin/slag-based zeolite microspheres geopolymer | 54.90 | [42] |
| Zeolitic materials | 144.0 | [50] |
| Hydroxyapatite embedded micro-adsorbents | 29.26 | [49] |

steps is the rate limiting step (the slowest step), intraparticle diffusion model [Eq. (8)] [51] was applied.

$$q_t = k_i t^{0.5} + C \tag{8}$$

where $k_i$ is the intraparticle diffusion rate effect and $C$ is a constant which gives the information on the effect of boundary layer, that is, larger intercept indicates that the external diffusion has a larger role as the rate limiting step. The values of $k_i$ and $C$ can be obtained from the plot $q_t$ vs. $t^{0.5}$. Intraparticle diffusion is the rate limiting step if the plot $q_t$ vs. $t^{0.5}$ is a straight line passing through the origin while deviation of the plot from linearity indicates the rate limiting step is film diffusion. The results presented in Fig. 6a indicate that the plot $q_t$ vs. $t^{0.5}$ consists of multilinear segments suggesting that multiple mechanisms were involved in the adsorption of $Sr^{2+}$ ions onto EAF slag. First linear segment indicates film diffusion, the second segment indicates intraparticle diffusion while the third segment indicates equilibrium stage. Since the second segments of plot $q_t$ vs. $t^{0.5}$ do not pass through the origin, adsorption of $Sr^{2+}$ onto EAF slag is not solely governed by intraparticle diffusion but by film diffusion as well [52].

Boyd's film diffusion model [53] [Eqs. (8)–(11)] was used deduce whether the film or particle diffusion controls the adsorption of $Sr^{2+}$ onto EAF slag,

$$F = 1 - \frac{6}{\pi^2}\sum_{n=1}^{\infty}\frac{1}{n^2}\exp\left(-n^2 B_t\right) \tag{9}$$

$$F = \frac{q_t}{q_e} \tag{10}$$

$$F = -0{,}4997 - \ln\left(1 - F(t)\right) \tag{11}$$

where $F$ is the fractional adsorption capacity at any given time and $B_t$ is a time constant which can be calculated at various temperature using Eq. (11). Intraparticle diffusion is the rate limiting step of the adsorption process if plot $B_t$ vs. $t$ has a straight line passing through the origin, while film diffusion mainly governs the adsorption process. The results presented in Fig. 6b indicate that film diffusion is the rate limiting parameter since none of the plots pass through the origin.

### 3.7. Adsorption thermodynamic

Thermodynamics of $Sr^{2+}$ adsorption onto EAF slag were evaluated using the following equations:

$$\Delta G° = \Delta H° - T\Delta S° \tag{12}$$

$$\Delta G° = -RT\ln K \tag{13}$$

$$\ln K_d = \frac{\Delta S°}{R} - \frac{\Delta H°}{RT} \tag{14}$$

$$K_d = \frac{\left(C_0 - C_e\right)\cdot V}{C_e \cdot m} \tag{15}$$

where $\Delta G°$, $\Delta H°$, $\Delta S°$ and $K_d$ present standard free energy enthalpy, entropy and equilibrium distribution coefficient, respectively. $C_o$ and $C_e$ are the initial and equilibrium concentrations of $Sr^{2+}$ ions in solution, respectively, $V$ is the volume of $Sr^{2+}$ ion solution and $m$ is the dry mass of adsorbent. The straight-line plots $\ln K_d$ vs. 1,000/$T$ (Fig. 7) enable determination of $\Delta H°$ and $\Delta S°$ values from the slope ($\Delta H°/R$) and intercept ($\Delta S°/R$), respectively.

The results presented in Table 6 indicate that adsorption of $Sr^{2+}$ onto EAF slag is endothermic in nature as the value of enthalpy is positive (44.9 kJ/mol). Moreover, this value falls in the range 40–200 kJ/mol which means that the $Sr^{2+}$ adsorption onto EAF slag involves chemisorption [54]. Negative values of free energy ($\Delta G°$) obtained at all investigated temperatures indicate that $Sr^{2+}$ adsorption onto EAF slag occurs spontaneously. The rise of temperature leads to the decrease of $\Delta G$ which indicates that the adsorption process is more favorable at higher temperatures.

### 3.8. SEM/EDS of EAF slag before and after adsorption

Adsorption of $Sr^{2+}$ onto the surface of slag particles is confirmed by SEM analysis in combination with EDS. Surface

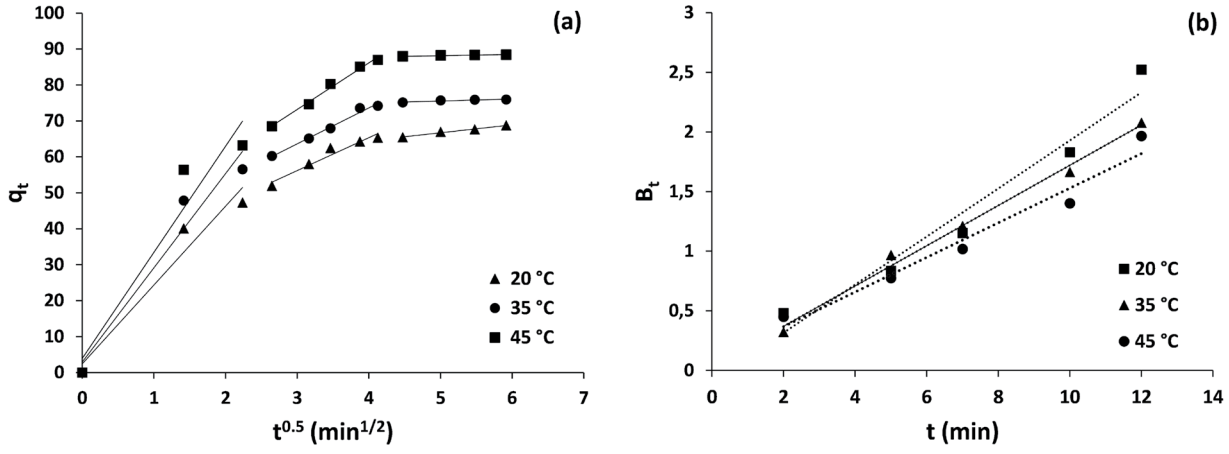


Fig. 6. Intraparticle diffusion plots (a) and plots $B_t$ vs. $t$ (b) for adsorption of $Sr^{2+}$ onto electric arc furnace slag at different temperatures.

morphology of sorbent particles before and after adsorption is given in Fig. 8a and b, respectively. EDS analysis of sorbent particles before adsorption (Fig. 7c), indicated presence of calcium, iron, silicon, aluminum and magnesium. In addition to these elements, the surface of sorbent after adsorption (Fig. 7d) was characterized by the presence of Sr.

## 4. Conclusions

In summary, EAF slag was used as an adsorbent for the $Sr^{2+}$ removal from aquatic solution. It has been characterized using XRPD and SEM/EDS. Moreover, particle size, porosity and point of zero charge ($pH_{pzc}$) of sorbent were also determined. The effects of contact time, pH, initial concentration of $Sr^{2+}$ and temperature on adsorption process were investigated. Kinetic, equilibrium and thermodynamic of adsorption process was evaluated as well. The results have shown that EAF slag, in relatively short time (15 min), was able to remove 68.75% of $Sr^{2+}$ in aquatic solution at 20°C, with initial concentration of $Sr^{2+}$ of 150 mg/L, adsorbent dosage of 1.5 g/L and pH of 5. Temperature increase enhances the $Sr^{2+}$ adsorption onto EAF slag and the highest removal efficiency of 88.40% was obtained at 45°C. Pseudo-first-order, pseudo-second-order models were applied on the experimental data to study kinetics of adsorption process. The results suggested that adsorption of $Sr^{2+}$ onto EAF slag proceeds according to the pseudo-second-order model. Langmuir and Freundlich isotherms were applied in order to evaluate equilibrium adsorption with the results elucidating that the equilibrium adsorption of $Sr^{2+}$ was best fitted to Langmuir isotherm suggesting that adsorption of $Sr^{2+}$ occurs on a homogenous surface of EAF slag covered by a monolayer of the adsorbate. Maximum adsorption capacity of EAF slag was 111.11 mg/g, surpassing already

Table 6
Thermodynamic parameters of $Sr^{2+}$ adsorption onto electric arc furnaces slag.

| Temperature (°C) | $K_d$ | $-\Delta G°$, (kJ/mol) | $\Delta H°$, (kJ/mol) | $\Delta S°$, (J/mol·K) |
|---|---|---|---|---|
| 20 | 1.25 | 0.55 | | |
| 35 | 2.76 | 2.59 | 44.9 | 156.3 |
| 45 | 5.51 | 4.51 | | |

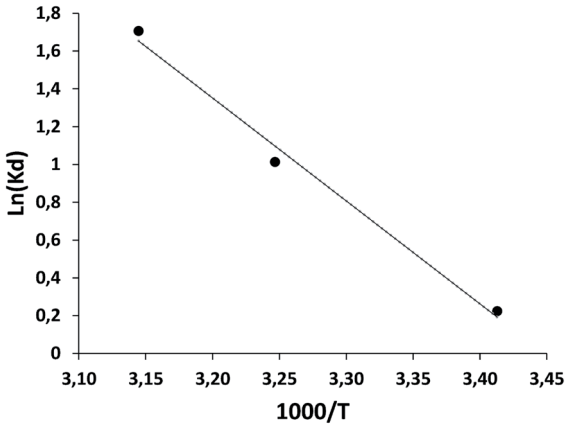


Fig. 7. Adsorption of $Sr^{2+}$ onto electric arc furnace slag as $\ln K_d$ vs. 1,000/$T$.

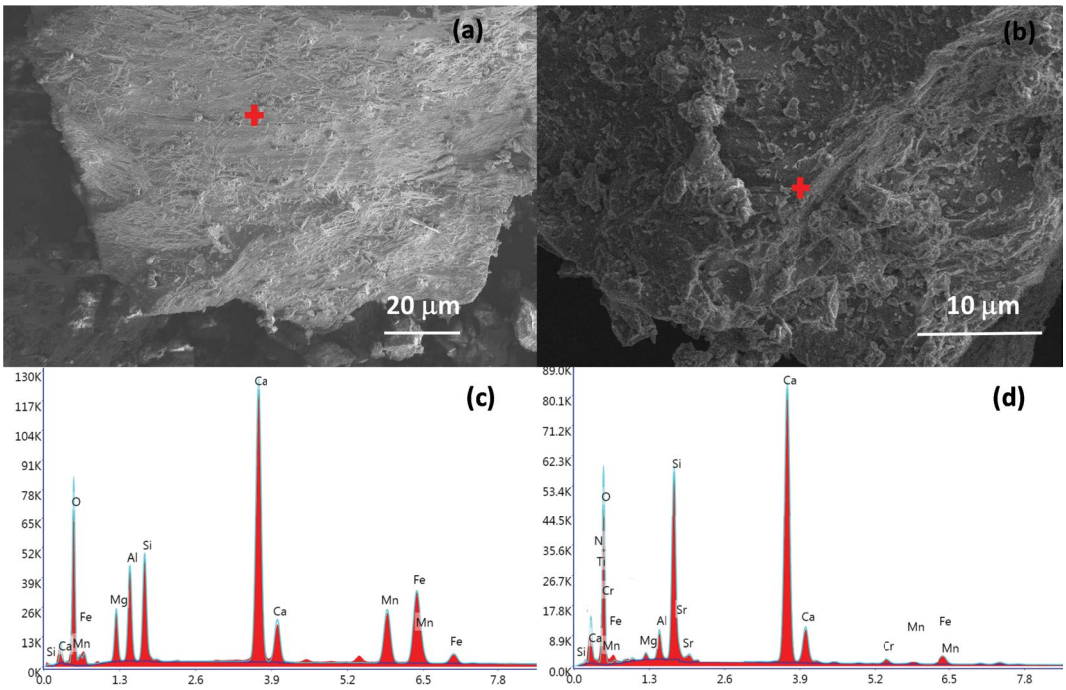


Fig. 8. Scanning electron microscopy of electric arc furnace slag before (a) and after adsorption (c) as well as energy-dispersive X-ray point analysis before (b) and after adsorption (d). The red cross notes the location of acquisition of energy-dispersive X-ray spectra.

reported materials such as dolomite, perlite, metakaolin and hydroxyapatite-based adsorbents. Adsorption mechanism was studied by applying intraparticle diffusion model and Boyd's film diffusion model and the results obtained indicated that film diffusion mainly governs the adsorption process. Thermodynamic investigations have indicated the endothermic character of $Sr^{2+}$ adsorption onto EAF slag since positive values of $\Delta H°$ were obtained. Moreover, adsorption process is spontaneous since negative values of $\Delta G°$ were obtained. These values decreased even further with an increase of temperature, suggesting a more favorable adsorption process at higher temperatures.

**Acknowledgements**

The authors would like to thank Dr. Smilja Marković and Dr. Ljiljana Veselinović from the Institute of Technical Sciences of SASA, Belgrade, Serbia, for technical support in XRPD and particle size investigations. The authors acknowledge Prof. Dr. Velimir Radmilović and from the Serbian Academy of Sciences and Arts and Prof. Dr. Vuk Radmilović from the Faculty of Technology and Metallurgy, University of Belgrade, Serbia for the help with microstructural investigation.

**References**

[1] A. Ahmadpour, M. Zabihi, M. Tahmasbi, T. Rohani Bastami, Effect of adsorbents and chemical treatments on the removal of strontium from aqueous solutions, J. Hazard. Mater., 182 (2010) 552–556.
[2] R. Apak, G. Atun, K. Güçlü, E. Tütem, Sorptive removal of Cesium-137 and strontium-90 from water by unconventional sorbents, J. Nucl. Sci. Technol., 33 (1996) 396–402.
[3] T. Kawamura, T. Ito, S.Y. Kim, Adsorption and separation behavior of strontium and yttrium using a silica-based CMPO adsorbent, J. Radioanal. Nucl. Chem., 320 (2019) 9–14.
[4] T. Kawamura, H. Wu, S.Y. Kim, Adsorption and separation behavior of strontium and yttrium using a silica-based bis(2-ethylhexyl) hydrogen phosphate adsorbent, J. Radioanal. Nucl. Chem., 329 (2021) 1001–1009.
[5] T.K. Rout, D.K. Sengupta, G. Kaur, S. Kumar, Enhanced removal of dissolved metal ions in radioactive effluents by flocculation, Int. J. Miner. Process., 80 (2006) 215–222.
[6] E.D. Hwang, K.W. Lee, K.H. Choo, S.J. Choi, S.H. Kim, C.H. Yoon, C.H. Lee, Effect of precipitation and complexation on nanofiltration of strontium-containing nuclear wastewater, Desalination, 147 (2002) 289–294.
[7] S.P. Mishra, D. Tiwary, Ion exchangers in radioactive waste management. Part XI. Removal of barium and strontium ions from aqueous solutions by hydrous ferric oxide, Appl. Radiat. Isot., 51 (1999) 359–366.
[8] Y. Cho, S. Komarneni, Cation exchange equilibria of cesium and strontium with K-depleted biotite and muscovite, Appl. Clay Sci., 44 (2009) 15–20.
[9] A.M. El-Kamash, M.R. El-Naggar, M.I. El-Dessouky, Immobilization of cesium and strontium radionuclides in zeolite-cement blends, J. Hazard. Mater., 136 (2006) 310–316.
[10] D.V. Marinin, G.N. Brown, Studies of sorbent/ion-exchange materials for the removal of radioactive strontium from liquid radioactive waste and high hardness groundwaters, Waste Manage., 20 (2000) 545–553.
[11] I. Smičiklas, S. Dimović, I. Plećaš, Removal of $Cs^{1+}$, $Sr^{2+}$ and $Co^{2+}$ from aqueous solutions by adsorption on natural clinoptilolite, Appl. Clay Sci., 35 (2007) 139–144.
[12] E. Başçetin, G. Atun, Adsorption behavior of strontium on binary mineral mixtures of montmorillonite and kaolinite, Appl. Radiat. Isot., 64 (2006) 957–964.
[13] C. Chen, J. Hu, D. Shao, J. Li, X. Wang, Adsorption behavior of multiwall carbon nanotube/iron oxide magnetic composites for Ni(II) and Sr(II), J. Hazard. Mater., 164 (2009) 923–928.
[14] Y.J. Tu, C.F. You, Z. Zhang, Y. Duan, J. Fu, D. Xu, Strontium removal in seawater by means of composite magnetic nanoparticles derived from industrial sludge, Water (Switzerland), 8 (2016) 2–12.
[15] X. Ye, T. Liu, Q. Li, H. Liu, Z. Wu, Comparison of strontium and calcium adsorption onto composite magnetic particles derived from $Fe_3O_4$ and bis(trimethoxysilylpropyl)amine, Colloids Surf., A, 330 (2008) 21–27.
[16] S. Chegrouche, A. Mellah, M. Barkat, Removal of strontium from aqueous solutions by adsorption onto activated carbon: kinetic and thermodynamic studies, Desalination, 235 (2009) 306–318.
[17] R. Rashid, I. Shafiq, P. Akhter, M.J. Iqbal, M. Hussain, A state-of-the-art review on wastewater treatment techniques: the effectiveness of adsorption method, Environ. Sci. Pollut. Res., 28 (2021) 9050–9066.
[18] Worldsteel, Worldsteel Association, Wordsteel Assoc., 2021. Available at: https://www.worldsteel.org/about-steel.html (Accessed August 28, 2022).
[19] Euroslag, Euroslag, Statistics, Euroslag, 2018. Available at: https://www.euroslag.com/products/statistics/statistics-2018 (Accessed August 28, 2022).
[20] I.Z. Yildirim, M. Prezzi, Chemical, mineralogical, and morphological properties of steel slag, Adv. Civ. Eng., 2011 (2011) 463638, doi: 10.1155/2011/463638.
[21] G. Song, L. Cao, X. Chen, W. Hou, Q. Wang, Heavy metal adsorption changes of EAF steel slag after phosphorus adsorption, Water Sci. Technol., 65 (2012) 1570–1576.
[22] M. Yusuf, F. Eghbali Babadei, S. Keshan Balavandy, B. Dastorian Jamnani, S. Hosseini, M. Rasool Malekbala, L. Abdullah Chuah, Removal of Ni(II) from aqueous solution by an electric arc furnace slag using artificial neural network approach, Adv. Environ. Biol., 7 (2013) 2303–2310.
[23] M. Yusuf, L. Chuah, M.A. Khan, T.S.Y. Choong, Adsorption of nickel on electric arc furnace slag: batch and column studies, Sep. Sci. Technol., 49 (2014) 388–397.
[24] L. Bláhová, Z. Navrátilová, M. Mucha, E. Navrátilová, V. Neděla, Influence of the slags treatment on the heavy metals binding, Int. J. Environ. Sci. Technol., 15 (2018) 697–706.
[25] H. Tang, W. Zhou, L. Zhang, Adsorption isotherms and kinetics studies of malachite green on chitin hydrogels, J. Hazard. Mater., 209–210 (2012) 218–225.
[26] I. Nikolić, D. Đurović, M. Tadić, V.V. Radmilović, V.R. Radmilović, Adsorption kinetics, equilibrium, and thermodynamics of $Cu^{2+}$ on pristine and alkali activated steel slag, Chem. Eng. Commun., 207 (2020) 1278–1297.
[27] A. Abu-Nada, A. Abdala, G. McKay, Isotherm and kinetic modeling of strontium adsorption on graphene oxide, Nanomaterials, 1 (2021) 2780, doi: 10.3390/nano11112780.
[28] G. Keçeli, Adsorption kinetics and equilibria of strontium onto kaolinite, Sep. Sci. Technol., 50 (2015) 72–80.
[29] A. Ghaemi, M. Torab-Mostaedi, M. Ghannadi-Maragheh, Characterizations of strontium(II) and barium(II) adsorption from aqueous solutions using dolomite powder, J. Hazard. Mater., 190 (2011) 916–921.
[30] J. Jang, D.S. Lee, Three-dimensional barium-sulfate-impregnated reduced graphene oxide aerogel for removal of strontium from aqueous solutions, J. Nucl. Mater., 504 (2018) 206–214.
[31] H. Amer, W.M. Moustafa, A.A. Farghali, W.M.A. El Rouby, W.F. Khalil, Efficient removal of cobalt(II) and strontium(II) metals from water using ethylene diamine tetra-acetic acid functionalized graphene oxide, Z. Anorg. Allg. Chem., 22 (2017) 1776–1784.
[32] T. Wen, X. Wu, M. Liu, Z. Xing, X. Wang, A.W. Xu, Efficient capture of strontium from aqueous solutions using graphene oxide-hydroxyapatite nanocomposites, Dalton Trans., 43 (2014) 7464–7472.
[33] C.R. Minitha, R. Suresh, U.K. Maity, Y. Haldorai, V. Subramaniam, P. Manoravi, M. Joseph, R.T. Rajendra Kumar,

Magnetite nanoparticle decorated reduced graphene oxide composite as an efficient and recoverable adsorbent for the removal of cesium and strontium ions, Ind. Eng. Chem. Res., 57 (2018) 1225–1232.
[34] N.A. Weerasekara, K.H. Choo, S.J. Choi, Metal oxide enhanced microfiltration for the selective removal of Co and Sr ions from nuclear laundry wastewater, J. Membr. Sci., 447 (2013) 87–95.
[35] A.M. El-Kamash, Evaluation of zeolite A for the sorptive removal of $Cs^{+}$ and $Sr^{2+}$ ions from aqueous solutions using batch and fixed bed column operations, J. Hazard. Mater., 151 (2008) 432–445.
[36] Y. Nishiyama, T. Hanafusa, J. Yamashita, Y. Yamamoto, T. Ono, Adsorption and removal of strontium in aqueous solution by synthetic hydroxyapatite, J. Radioanal. Nucl. Chem., 307 (2016) 1279–1285.
[37] N.O. Yigit, S. Tozum, Removal of selenium species from waters using various surface-modified natural particles and waste materials, Clean – Soil Air Water, 40 (2012) 735–745.
[38] S. Brunauer, P.H. Emmett, E. Teller, Adsorption of gases in multimolecular layers, J. Am. Chem. Soc., 60 (1938) 309–319.
[39] E.P. Barrett, L.G. Joyner, P.P. Halenda, The determination of pore volume and area distributions in porous substances. I. Computations from nitrogen isotherms, J. Am. Chem. Soc., 73 (1951) 373–380.
[40] J. Gulicovski, L. Cerovic, S. Milonjic, Point of zero charge and isoelectric point of alumina materials and manufacturing processes, Mater. Manuf. Processes, 23 (2008) 615–619.
[41] F.Y. Wang, H. Wang, J.W. Ma, Adsorption of cadmium(II) ions from aqueous solution by a new low-cost adsorbent-bamboo charcoal, J. Hazard. Mater., 177 (2010) 300–306.
[42] H. Lei, Y. Muhammad, K. Wang, M. Yi, C. He, Y. Wei, T. Fujita, Facile fabrication of metakaolin/slag-based zeolite microspheres (M/SZMs) geopolymer for the efficient remediation of $Cs^{+}$ and $Sr^{2+}$ from aqueous media, J. Hazard. Mater., 406 (2021) 124292, doi: 10.1016/j.jhazmat.2020.124292.
[43] M. Uysal, I. Ar, Removal of Cr(VI) from industrial wastewaters by adsorption. Part I: determination of optimum conditions, J. Hazard. Mater., 149 (2007) 482–491.
[44] S.S. Baral, S.N. Das, P. Rath, Hexavalent chromium removal from aqueous solution by adsorption on treated sawdust, Biochem. Eng. J., 31 (2006) 216–222.
[45] S. Bevara, P. Giri, S.N. Achary, G. Bhallerao, R.K. Mishra, A. Kumar, C.P. Kaushik, A.K. Tyagi, Synthetic Na/K-birnessite for efficient management of Sr(II) from nuclear waste, J. Environ. Chem. Eng., 6 (2018) 7200–7213.
[46] A.I. Matskevich, E.A. Tokar', N.P. Ivanov, T.A. Sokolnitskaya, Y.A. Parot'kina, A.N. Dran'kov, V.E. Silant'ev, A.M. Egorin, Study on the adsorption of strontium on granular manganese oxide, J. Radioanal. Nucl. Chem., 327 (2021) 1005–1017.
[47] M. Jain, V.K. Garg, K. Kadirvelu, Adsorption of hexavalent chromium from aqueous medium onto carbonaceous adsorbents prepared from waste biomass, J. Environ. Manage., 91 (2010) 949–957.
[48] M. Torab-Mostaedi, A. Ghaemi, H. Ghassabzadeh, M. Ghannadi-Maragheh, Removal of strontium and barium from aqueous solutions by adsorption onto expanded perlite, Can. J. Chem. Eng., 89 (2011) 1247–1254.
[49] B. Park, S.M. Ghoreishian, Y. Kim, B.J. Park, S.M. Kang, Y.S. Huh, Dual-functional micro-adsorbents: application for simultaneous adsorption of cesium and strontium, Chemosphere, 263 (2021) 128266, doi: 10.1016/j.chemosphere.2020.128266.
[50] M.G. Lee, S.K. Kam, C.H. Lee, Kinetic and isothermal adsorption properties of strontium and cesium ions by zeolitic materials synthesized from jeju volcanic rocks, Environ. Eng. Res., 26 (2021) 200127, doi: 10.4491/eer.2020.127.
[51] W. Weber, J. Morris, Kinetics of adsorption on carbon from solution, J. Sanit. Eng. Div., 89 (1963) 31–60.
[52] D. Kumar, J.P. Gaur, Chemical reaction- and particle diffusion-based kinetic modeling of metal biosorption by a Phormidium sp.-dominated cyanobacterial mat, Bioresour. Technol., 102 (2011) 633–640.
[53] G.E. Boyd, A.W. Adamson, L.S. Myers, The exchange adsorption of ions from aqueous solutions by organic zeolites. II. Kinetics, J. Am. Chem. Soc., 69 (1947) 2836–2848.
[54] M.R. Yazdani, T. Tuutijärvi, A. Bhatnagar, R. Vahala, Adsorptive removal of arsenic(V) from aqueous phase by feldspars: kinetics, mechanism, and thermodynamic aspects of adsorption, J. Mol. Liq., 214 (2016) 149–156.